ADVANCED MATERIALS TECHNOLOGIES
www.advmattechnol.de

A Stretchable Strain Sensor System for Wireless Measurement of Musculoskeletal Soft Tissue Strains

Qiang Zhang, Fransiska M. Bossuyt, Naomi C. Adam, Byron Llerena Zambrano, Flurin Stauffer, Patrick Rennhard, Roman Gubler, Roland Küng, Sarah Abramovic, Vullnet Useini, Walter Herzog, Tim Leonard, Michael W. Scott, William R. Taylor, and Colin R. Smith*

Measurement of in vivo strain patterns of musculoskeletal soft tissues (MSTs) during functional activities reveals their biomechanical function, supports the identification and understanding of pathologies, and quantifies tissue adaptation during healing. These scientific and clinical insights have motivated the development and application of various strain sensors to quantify MST strains in either intraoperative or dynamic in vivo conditions. In this study, a strain sensor system is developed based on stretchable electronics and radio frequency identification technologies. In this system, a flexible inductor-capacitor-resistor sensor is fabricated such that it can be wirelessly excited by a custom-designed readout box through electronic resonance. The resonant frequency of the sensor changes when the capacitor is stretched, which is then also recorded by the readout box at a sampling rate of 1024 Hz. Suturing the stretchable capacitor onto the MST allows it to be stretched in line with musculoskeletal deformations, hence providing an indirect method to assess strain patterns in vivo. Application of the system ex vivo indicates that the signal remains linear between 0 and 25% strain and is electronically stable in a simulated in vivo environment for one week and over 100 000 cycles of fatigue loadings. The strain sensor exhibits excellent resolution (0.1% strain, ≈9 µm) during wireless strain measurement. Finally, sensor implantation and strain measurement onto the medial gastrocnemius tendon of a sheep indicate that the sensor is able to record repetitive strain patterns in vivo during dynamic movements. This study indicates the potential scientific and clinical applicability in vivo.

1. Introduction

Musculoskeletal soft tissues (MSTs) such as ligaments and tendons play a key role in absorbing external impacts,[1] stabilizing joints,[2] and providing joint proprioception.[3] Injuries to MSTs can limit musculoskeletal function and initiate tendinopathy and osteoarthritis in neighboring tissues, and thus detrimentally impact quality of life.[4–6] Successful treatment of MST injuries relies on a comprehensive understanding of the functional demands of MSTs during dynamic activities, as well as during healing and/or adaptive response of a tissue to loading. Estimations of in vivo tendon strains using ultrasound techniques have attempted to reveal the complex interactions within muscle-tendon units that transmit energy from muscle contraction, amplify power output, and absorb shocks during impact.[7,8] However, such estimates have several limitations including, but not limited to, controversial reliability and confounding out-of-plane motion,[9] hence indicating the need for direct measurements of tendon strain. Measurements of in vivo ligament

Q. Zhang, N. C. Adam, S. Abramovic, V. Useini, W. R. Taylor, C. R. Smith
Institute for Biomechanics
ETH Zürich
Zürich 8093, Switzerland
E-mail: bt@ethz.ch

F. M. Bossuyt, W. Herzog, T. Leonard
Human Performance Lab
University of Calgary
Calgary 2500, Canada

F. M. Bossuyt
Shoulder Health and Mobility Group
Swiss Paraplegic Research
Nottwil 6207, Switzerland

B. L. Zambrano, F. Stauffer
Laboratory of Biosensors and Bioelectronics
ETH Zürich
Zürich 8092, Switzerland

P. Rennhard, R. Gubler, R. Küng
Institute of Signal Processing and Wireless Communications
ZHAW School of Engineering
Winterthur 8401, Switzerland

M. W. Scott
Faculty of Veterinary Medicine
University of Calgary
Calgary 3280, Canada

The ORCID identification number(s) for the author(s) of this article can be found under https://doi.org/10.1002/admt.202202041

DOI: 10.1002/admt.202202041

strains during various activities have supported the optimization of rehabilitation protocols to stimulate anterior cruciate ligament healing and avoid damage,[10,11] but have also aided in the evaluation of total knee arthroplasty techniques and component designs on soft tissue loading and pathological adaptions.[12,13] The quantification of in vivo MST strains is therefore critical for both facilitating scientific discoveries on tissue function and driving innovative clinical treatments. To this end, implantable strain sensors can be physically attached to the ligament and tendon to convert deformation of the tissue into sensor electrical signals,[14] and thus enable in vivo strains to be measured in humans with high accuracy and sampling rates.[14–16] Importantly, such approaches provide sufficient robustness, minimal tissue disruption, wireless data transmission, and long-term biocompatibility, and are therefore able to withstand the demands of *in-vivo* MST strain measurements during dynamic activities, including repeated and rapid tissue deformations (i.e., strain rates up to 50% s^{-1} in Achilles tendons).[17]

Various implantable sensors have been used to measure MST strains in vivo, but previous measurements in humans have almost exclusively been limited to intraoperative environments and widespread application of strain sensors in patients has not been achieved due to limitations in sensor designs. As an example, magnetic field sensors, such as Hall effect strain transducers and differential variable reluctance transducers, have been implanted onto the anterior cruciate ligament (ACL) of human subjects to measure ACL strains throughout a variety of movements such as squatting and bicycling.[11,18] However, several disadvantages limit these sensor designs for in vivo MST strain measurements. First, the rigid construction of these sensors often leads to sensor impingement with neighboring musculoskeletal tissues, which limits the tissues and postures that can be measured.[16] Second, the fixation methods adopted by these sensors are suboptimal for dynamic measurements of MST strains. Magnetic field sensors can be fixed through pressing two barbs of the sensor into the tissue,[19,20] but the security of the fixation during dynamic measurements may be weak. It is important to note, however, that these sensors require a cable to transmit the measurement signal,[19,21,22] and thus an open transcutaneous incision limits the applicability to both human and animal experiments. Finally, bending of the cable can induce artefacts in the sensor signal.[23] Thus, many clinically important MST strain measures could become masked, indicating that the need for a novel sensor technology that enables long-term dynamic in vivo measurements remains unmet.

Recent advances in stretchable electronics have facilitated the development of membrane-like stretchable strain sensors with great potential for clinical application through their unique soft constitutions that can easily conform to the surface morphologies of tissues and thus minimize sensor impingement. These sensors have shown outstanding conductivity, stretchability, and durability,[24–26] and have been used to track human body movements,[27–31] measure human bladder volume,[32,33] and monitor heart rate.[34] These sensors are typically fabricated by embedding conductive materials in stretchable elastomers, and can be generally classified into resistive-type sensors consisting of a single conductive layer [29,31,35] or capacitive-type sensors with two conductive layers.[30,33,36] In a capacitive-type sensor, the capacitance increases upon stretching due to thinning of the dielectric layer and shape variation of the overlapping area.[37,38] These sensors exhibit low hysteresis, less overshoot, and higher linearity in electromechanical response compared to their resistive-type counterparts.[37,39,40] Despite the disruptive technology in implantable strain sensors, to our knowledge, very few stretchable strain sensors have been employed to quantify MST strains.[41,42] Zens and co-workers used a capacitive-type sensor to measure anterolateral ligament strains on a knee specimen.[42] Boutry and co-workers developed a biodegradable sensor that enables the monitoring of long-term MST strains.[43] However, the sensors were glued on the tissues during measurement, which may lead to tissue damage and biocompatibility issues. A full demonstration of these elastomer-based strain sensors to endure long-term and high-rate fatigue loadings also remains lacking. Importantly, the sensor techniques of both research groups failed to incorporate percutaneous wireless data transmission, which could be realized through wireless sensors that use on-board batteries,[44,45] near field communication technology,[34] or antenna coils.[33,37,46]

In this study, we introduce an advanced stretchable sensor system with calibration methodology, and provide a comprehensive demonstration of the strain measurement capacity in both ex vivo and simulated in vivo environments. In our sensor, the stretchable capacitor has been used for wireless signal transmission by simply adding a coil to the capacitor to create a chipless inductor-capacitor-resistor (LCR) sensor that can be wirelessly powered and monitored via an external readout.[33,47] The system was designed to be directly sutured onto MSTs in the body, while a novel wearable readout wirelessly powered and measured the sensor signal from the outside of the body. An iPad Operating System app controls the system and displays sensor data in real-time. The system can simultaneously measure multiple sensors attached to different tissues, meaning that it can quantify the coordinated function of multiple passive restraints in a joint. The sensor has outstanding resolution for wireless strain measurement (0.1% strain, ≈9 μm), and remains reliable over 100 000 cycles of fatigue loadings. We performed ex vivo sensor measurements on a sheep plantaris tendon to illustrate the potential of the sensor system for dynamically quantifying the strain of soft tissues. Furthermore, we characterized the in vivo function of the sensor on the medial gastrocnemius tendon in a freely moving sheep to demonstrate the potential applicability of the sensor system for characterizing in vivo function of soft tissues during locomotion.

2. Results

2.1. Sensor Design and Properties

The strain sensor system consists of an implantable strain sensor and a portable readout box (**Figure 1**). The sensor was fabricated as a stretchable capacitor containing two layers of conductive gold titanium dioxide nanowires (Au-TiO_2 NW) separated by a layer of dielectric silicone rubber, resembling a membrane-like "sandwich" plate structure that is embedded in biocompatible polydimethylsiloxane (PDMS) (Figure 1a–c). A detailed explanation on the working principle of the plate capacitor could be found in the Supporting Information. The capacitor is bonded to a coil inductor to form a LCR circuit, which is then cast in PDMS to construct the whole sensor. Thus, the sensor can be

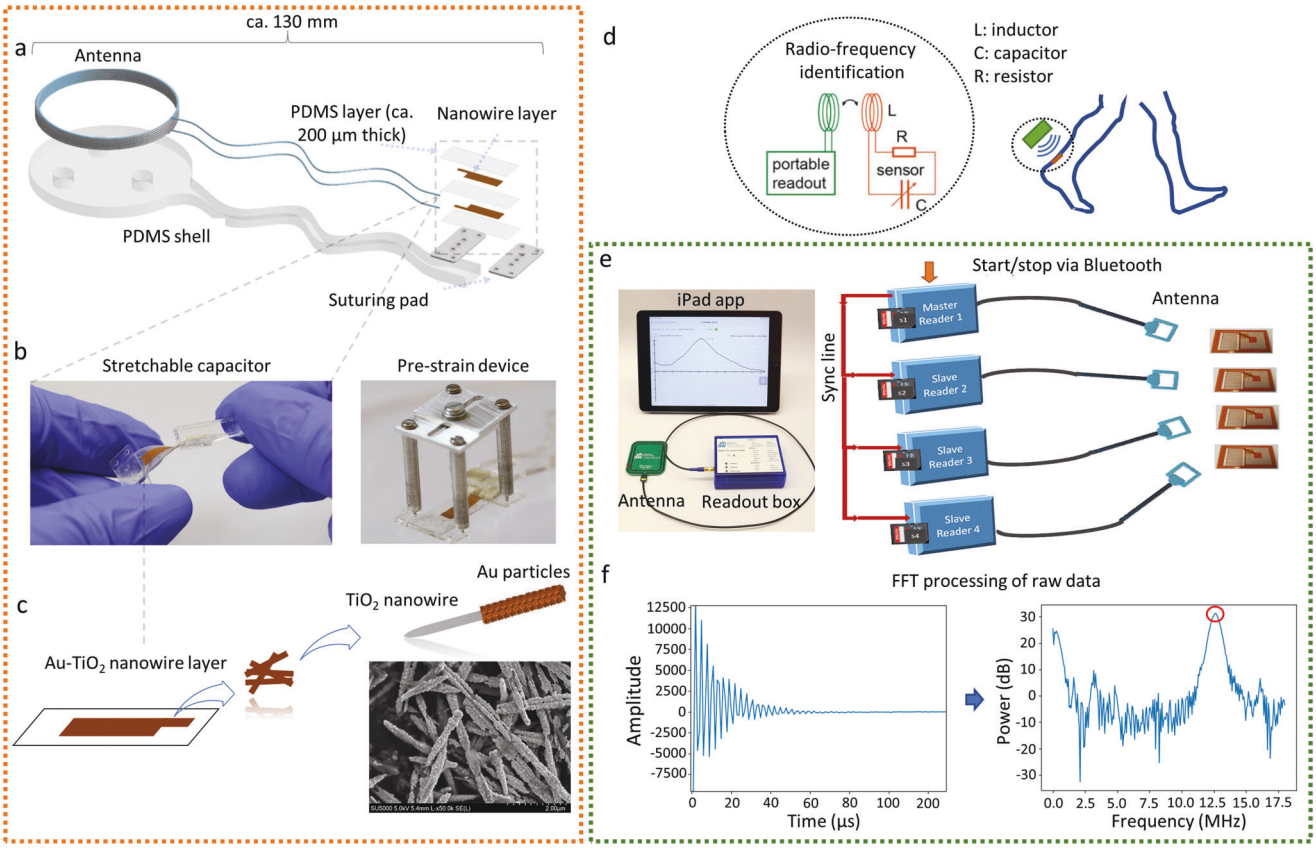

Figure 1. Wireless sensor technology for in vivo measurement of musculoskeletal soft tissue strain. a) Scheme of the stretchable strain sensor, b) left: stretchable capacitor; right: pre-strain device for pre-stretching the sensor during implantation so that the sensor can also measure shortening, c) conductive layer patterned with Au-TiO_2 nanowires, d) scheme of in vivo wireless strain measurement based on radio-frequency identification technology, e) left: sensor readout system including a readout box with antenna and an iPad app for controlling and displaying real-time sensor signals; right: synchronization of multiple readout boxes and start/stop control via Bluetooth, and f) the raw data are processed with a FFT (512 points) to obtain the resonant frequency.

modelled by three passive components: L is the inductance of the sensor coil, C is the proper sensing element, and R represents the sensor's signal losses (Figure 1d). A pulse signal is sent from a custom-designed (Figure 1e) readout system to excite the LCR sensor, and the response signal feedback is collected and spectrally analyzed to obtain its resonant frequency (RF). Specifically, a continuous sine wave signal is first sent from the transmitting coil in the transmit phase to the sensor coil using near field magnetic coupling. The LCR sensor is energized at the same time through the coupling in a forced oscillation, which has the same frequency as the excitation sine wave. After turning off the transmitter signal, the receive phase starts immediately. An exponentially decaying oscillation of the sensor signal (Figure 1f) can be measured through the detecting receiver coil, which is in fact the transmitter coil switched without causing transients to the receive circuitry. The frequency immediately changes from forced to self-resonance frequency, which is given by the LCR sensor's RF.

As the sensing component of the sensor, the stretchable capacitor demonstrated excellent electronic performance during ex vivo tensile tests. The capacitance increased with high linearity ($R^2 > 0.99$) under axial strains from 5% to 20% (Figure S1, Supporting Information). The capacitor also had outstanding resolution, detecting strains down to 0.1% (≈9 µm). Moreover, the linearity and resolution of the capacitor remained unchanged after 100 000 cyclic loadings (Figure S1, Supporting Information). The sensor could be stitched onto the tissue using surgical sutures in order to provide a secure fixation. To prevent damage to the soft component during suturing, two rigid suturing pads were fabricated and fixed onto the capacitor. A custom-designed pre-strain device (Figure 1b) then held the sensor at a pre-strain of ≈15% during suturing, hence providing stability during surgery.

Simultaneous measurement of multiple sensors was enabled by internally synchronizing different readout boxes with time packets sent from a "master" readout box to nearby "slave" readout boxes via Bluetooth (Figure 1e). This function allows strains in multiple MSTs or different bundles of a MST to be concurrently recorded, enabling the investigation of the coordination of multiple MSTs during dynamic movements. However, in order to avoid signal interference, the distance between antenna of each sensor should be at least 10 cm (even though sensor capacitors can be located closer to one another). Moreover, the sensor system can be synchronized to other measurement devices (e.g., motion capture system and inertial measurement units) with a custom-designed synchronization box that can send and record digital and analog pulses. The sensor system is controlled by an

iPad-based app via a Bluetooth connection (Figure S2, Supporting Information). The received data is transmitted to the readout box for Fast Fourier Transformation (FFT, 512 points, Figure 1f) and display of the real-time RF of each sensor, which is also stored on a Secure Digital card for further data analysis.

2.2. Wireless Sensing Performance

The measured RF decreased with increasing strain applied to the sensor (**Figure 2**a,b). Similarly, the Q-factor, a measure of signal energy preservation within the sensor system, decreased with increasing strain. When repeated cycles were performed in the tensile testing machine, the RF signal was highly repetitive (Figure 2b), suggesting that the sensor had almost negligible viscoelastic properties.

For the sensor resolution test in air, 0.1% strain (≈9 μm) applied by the tensile testing machine led to an observable change in the RF of the sensor (Figure 2c). Similar tests in phosphate buffered saline (PBS) aimed to simulate the in vivo environment, which demonstrated comparable resolutions of the sensor system as the tests in air. Importantly, the pre-strain level played no clear role on the signal-to-noise ratio (SNR) of the sensor system. In air, the sensor had a larger SNR at 15% pre-strain level compared to 10% and 5%. In PBS, however, the sensor signal was slightly noisier at higher pre-strain levels, where the SNR was smaller at 15% pre-strain than at 10% and 5% pre-strains (Figure 2c). Finally, regardless of the testing conditions, small overshoots were observed while 0.5% strains were applied (Figure 2c). Finally, the sensor RF signal was measured during stepwise loadings, both in air and in PBS. For the test in air, the RF of the sensor gradually decreased from 13.80 to 12.53 MHz with strain increasing from 0 to 25% (Figure 2d). When the sensor was submerged in PBS, the 0%-strain RF of the sensor decreased to 12.98 MHz and further decreased to 11.73 MHz at 25% strain.

2.3. Ex Vivo Testing

The wireless sensing properties of the sensor system was tested in a simulated in vivo environment (PBS, 37 °C) for one week, in order to assess possible changes that occur in the body. Here, the RF of the sensor decreased ≈1 MHz one day after being immersed in PBS (**Figure 3**a), while the Q-factor of the sensor considerably decreased from 35.9 to 18.7. In additional tests to establish the influence of temperature on the sensor signals, the RF of the sensor increased from 13.863 to 14.025 MHz with a temperature rise from 22 to 45 °C in a linear manner (Figure 3b).

To demonstrate the sensors applicability for measuring strains in MSTs, the sensor was sutured to a cadaveric sheep plantaris tendon for cyclic loading in a tensile testing machine (Figure 3c). Here, repetitive cycles of tissue strains were successfully recorded at 1024 Hz throughout testing (Figure 3c). Following calibration of the sensor RF to the length changes measured with sonomicrometry crystals located underneath the sensor, the RF variations indicated an average of 4.2% strain in the tendon throughout the 51 loading cycles.

2.4. In Vivo Sensor Implantation in Sheep and Dynamic Measurement of Medial Gastrocnemius Tendon Biomechanics

First proof-of-concept in vivo tendon strain measurements during locomotion were conducted after implanting a calibrated strain sensor onto the medial gastrocnemius tendon of a sheep. In addition, a custom-made "E"-shaped buckle-type force transducer[49] was implanted on the same tendon to measure the muscle forces of the medial gastrocnemius on the tendon (**Figure 4**a). For 2 d following implantation, the sheep was able to fully weight bear, and with appropriate analgesic, showed only minimal signs of limping on the instrumented leg. Three days postoperatively, the sheep performed trotting tests on a treadmill at 1.34 m s^{-1}, during which continuous strain and force measurements were undertaken (Figure 4b). Toe-off event occurred at 41% of the total stride time on average. A maximum strain of 3.8% was observed during the stance phase of the trotting cycle.

3. Discussion

This study aimed to develop a wireless strain sensor system and validate its functionality for in vivo measurement of MST strains. With a LCR circuit design, the RF of the sensor varies according to the sensor capacitance, which changes when strain is applied.[33] Once the capacitor is fixed onto MST, the local tissue strain can be quantified according to the RF of the sensor, which is wirelessly captured by the readout box at a sampling rate of 1024 Hz based on induction coupling of the antennas.[33,50] A time domain method[51] was employed for the readout box design, in order to realize such a high sampling rate of the measurements. Without the need for a transdermal cable, the implantation skin incision can heal and mitigate potential interruptions from cable migration on the signal quality, hence allowing the high-rate wireless sensing system to track MST strains during dynamic body movements.

We used Au-TiO_2 NWs as the electrode material of the sensor, since PDMS composites with Au-TiO_2 NWs are known to be biocompatible.[48] Importantly, our readout system is only able to measure wireless signals with sufficient quality, which only occurs when the sensor's Q-factor remains above 10, meaning that an excessive decay of the Q-factor due to a strain-induced increase of electrode resistance should be prevented. The conductive coating with Au nanoparticles was able to greatly improve the conductivity of the electrodes. The sheet resistance of Au-TiO_2 NW electrodes embedded in PDMS was found to remain below 10 Ω $\square^{-1}$ at strains of up to 100%.[48] This allowed us to fabricate the LCR sensor with an ideal Q-factor, resulting in improved signal quality in wireless sensing measurements. In this study, the Q-factor of the sensor was assessed in the tensile test. The results showed that the Q-factor of the sensor decreased with increasing series resistance of the nanowire layers in the capacitor under strained conditions,[56,57] but that a Q-factor of 10 or greater can be achieved at strains of up to, and even slightly beyond 25% strain. The sensor exhibited excellent performance and resolution when tested up to 25% strain in a tensile testing machine. Since macroscopic failure of MSTs is known to occur at strains of 8%–15% ex vivo,[52–55] the 25% strain range achievable by the sensor allows a sufficient range for characterization of MST strains. In addition, our LCR sensor was fabricated with PDMS. PDMS

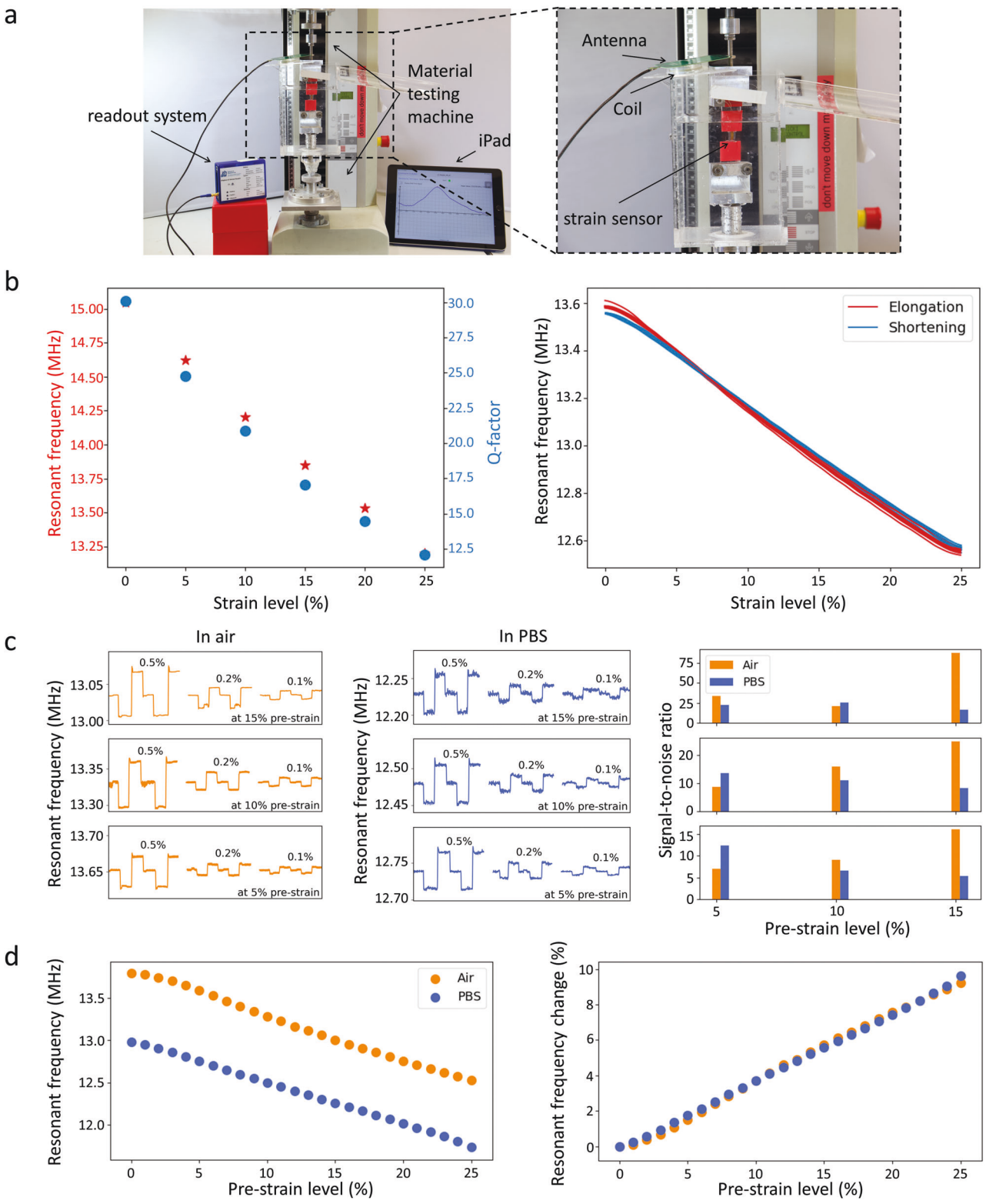

Figure 2. Wireless measurement performance of the strain sensor: a) Experimental setup for wireless measurements with the zoomed region highlighting the tensile testing machine with strain sensor and readout antenna, b) left: changes of sensor resonant frequency and Q-factor against strains from 0 to 25%; right: low hysteresis effect of the sensor under cyclic loadings, c) left: two out of ten cycles of ±0.5%, ±0.2%, and ±0.1% strain steps at different pre-strain levels in air; middle: two out of ten cycles of ±0.5%, ±0.2%, and ±0.1% strain steps at different pre-strain levels in PBS; right: corresponding signal to noise ratio for both air and PBS conditions, and d) left: absolute resonant frequency changes with strain from 0% to 25% in air and PBS; right: relative resonant frequency changes with strain from 0% to 25% in air and PBS.

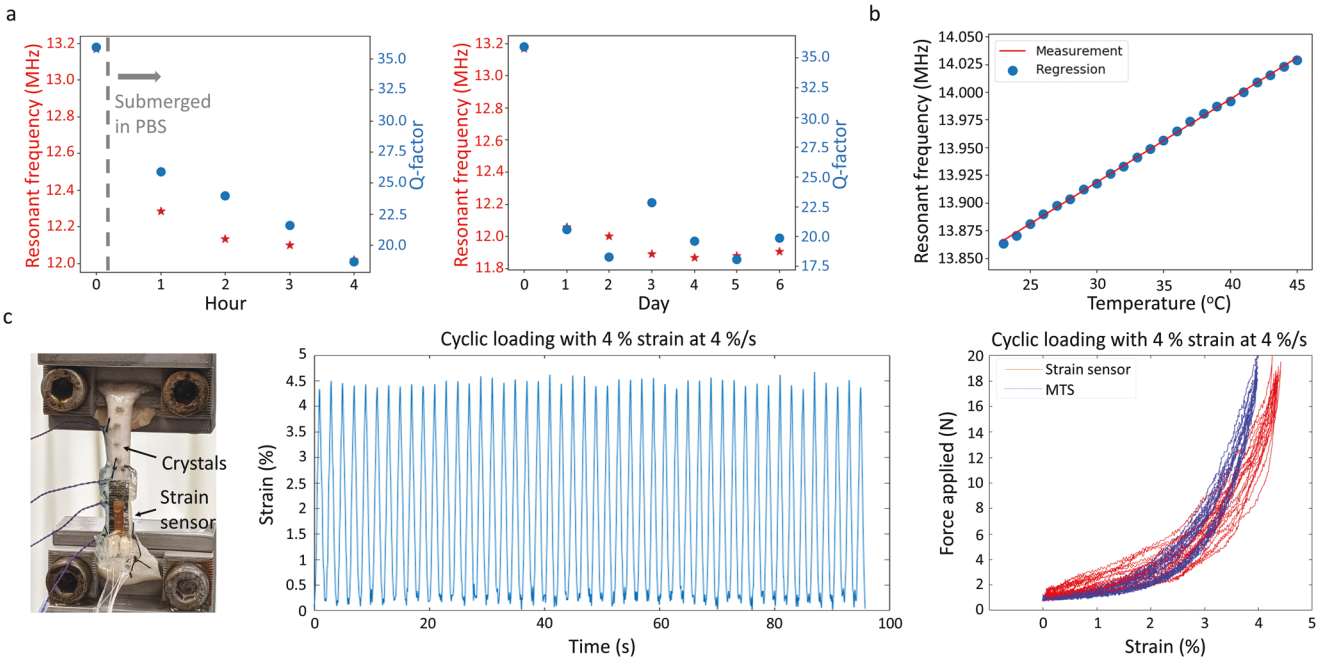

Figure 3. Ex vivo validation and measurements of the LCR sensor. a) Left: Changes of sensor resonant frequency and Q-factor in a simulated in vivo environment in the first 4 h; right: changes of sensor signal in the following week, b) linear increase of the sensor resonant frequency with a temperature increase from 23 to 45 °C, and c) left: ex vivo strain measurement of a sheep plantaris tendon; middle: repetitive change of measured strain during 51 loading cycles; right: tendon strains assessed by the sensor compared to the strains applied by the tensile testing machine (MTS).

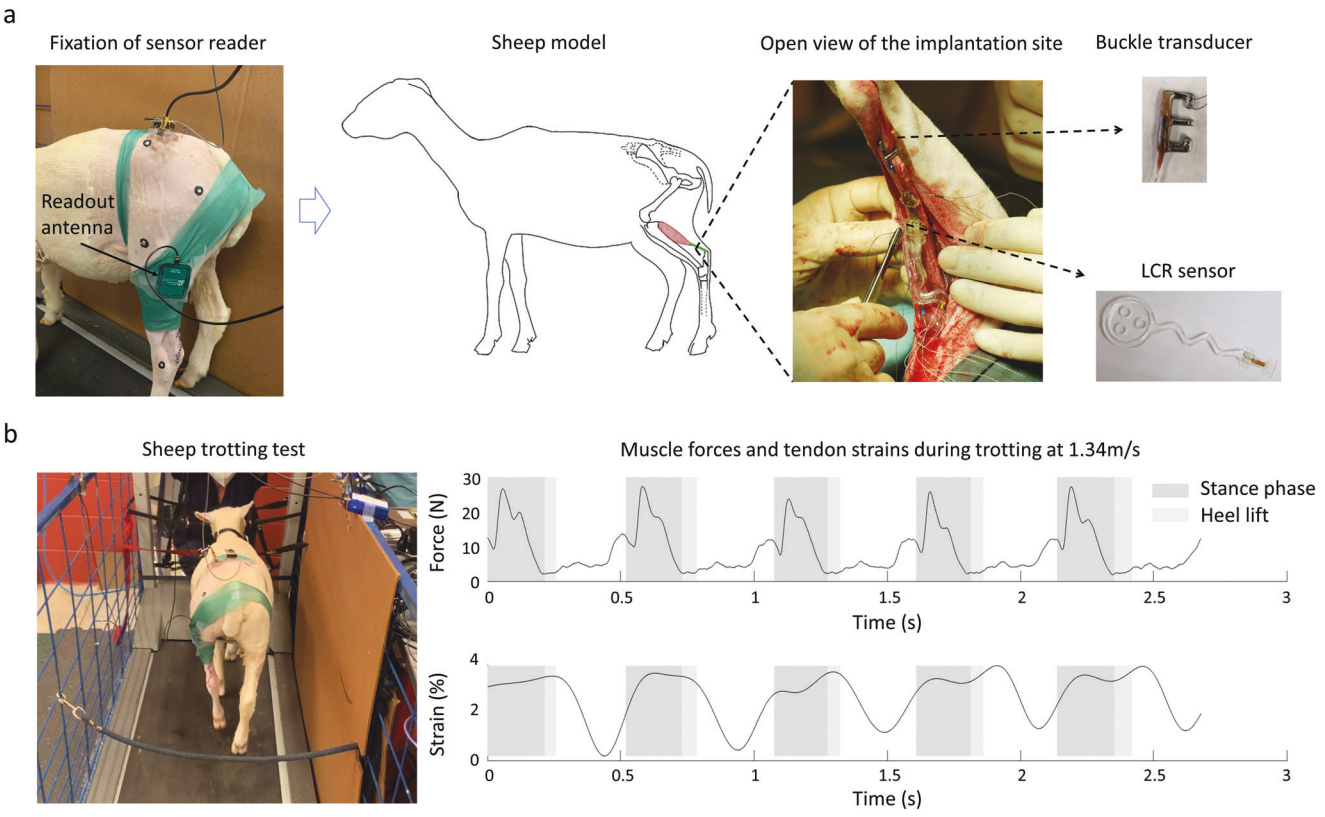

Figure 4. In vivo sensor implantation and strain measurement. a) Sheep instrumenting, implantation site, and sensors, and b) left: sheep trotting test on a treadmill; right: the force and strain of sheep medial gastrocnemius tendon during trotting.

has a Young's modulus of 1–2 MPa,[58] which is much smaller than MSTs such as human tendons (1.2 GPa)[59] and muscle fascia (71.6–275.9 MPa).[60] Therefore, the sensor capacitor has a sufficiently high compliance to the natural elongations of MSTs. As such, this approach lends itself ideally to the assessment of MST strains in the human body.

High resolution in wireless sensing is considered to be a critical prerequisite of the sensor system for scientific and clinical applications.[15,16,61] In this study, we demonstrated that the sensor system has an excellent resolution of 0.1% strain in both in air and in PBS. System sensitivity to small strain perturbations was confirmed in mechanical tests. In previous studies, strain sensors including wired data transmissions were reported to have signal resolution of around 0.5%.[16,41,42] For wireless data transmission, good signal resolution can be achieved by using active sensors with internal power sources to send reinforced signals.[44] In this study, however, the strain sensor was chipless and utilised passive data transmission, but still achieved the high quality and resolution of its active counterparts. Additional benefits of our wireless approach include structure simplicity for in vivo implantation and low risk of biological reactions to active components.

As the strain sensor will be surgically sutured at an unknown length during implantation, the effect of sensor pre-strain levels on the resolution of the sensor system was studied by comparing the SNR of the sensor. A low correlation between the pre-strain level (5%–15% strains) and sensor SNR was observed, indicating that the pre-strain level is not critical for measurements as long as it remains within the testing range. In addition, overshoot of the sensor RF signal was observed in the resolution test, which can be explained by the specific material response of polymers used, as well as non-uniform movement between the solid nanowires and polymer molecules.[24,40,62,63] In this study, the signal overshoot was not observed at smaller strain steps (0.1% and 0.2%), suggesting that the magnitude of overshoot may be dependent on the level of strain applied to the sensor. The relationship between overshoot and strain was also observed in another study, where Rahimi and co-workers found that their stretchable resistor showed larger overshoot at strains over 50% compared to lower strains.[64]

For MST strain measurement, the sensor should be calibrated to axial strain before implantation. However, the observed decrease of sensor RF due to the change of testing condition indicates that ex vivo sensor calibration cannot be used to assess the absolute length of the instrumented region in the MST, even post-measurement. In our study, the relative change of the sensor RF with strain was almost identical in both air and PBS environments, with each achieving a similar average gauge factor[33] of 0.38 (Figure 2d). This finding is important for in vivo strain measurements, since the ex vivo sensor calibration is still a reliable method to assess the relative length change (strain) of the MST measured. The consequences for practical application, and a possible limitation of system usage, are that strains can only be measured relative to a standardized posture or pose. As such, a position that can be reliably replicated (e.g., relaxed supine) should be used in order to provide a suitable reference state.

The sensor exhibited a decrease in RF after being immersed in PBS. These changes are likely due to the increased sensor capacitance caused by PBS absorption, which was also reported in a previous study.[65] PBS absorption of PDMS is known to increase the parasitic capacitance between the nanowire electrode and electrolyte through the PDMS.[66] Importantly, sensor RF and Q-factor plateaued approximately 1 d after immersion, suggesting that the signal of the sensor could be stable over a longer period of time in the living body. In addition, the effect of temperature on wireless sensing properties was evaluated because of possible body temperature changes during activities in vivo.[67] According to the outcomes of our measurement, it could be predicted that across a temperature range of 38–40 °C, the RF of the sensor may slightly change (average 0.011 MHz), which accounts for an error of less than 0.2%. The sensor's resonant frequency (RF) might increase due to thermal expansion of the PDMS[68] (detailed explanation in the Supporting Information). Importantly, this error can be mostly mitigated by in vivo pre-conditioning (i.e., warm-up walking) before measurement.

During the ex vivo tensile tendon test, an average strain of 4.2% in the sheep plantaris tendon was measured by the strain sensor system, which was slightly larger than the 4.0% strain applied by the tensile testing machine. It should be noted that the tensile testing machine measures the overall length changes of the complete tendon, while the sensor measures a sub-region of the tendon near the lower clamping site. While specimen geometry and local material properties can clearly play a role on localized strain distributions, it has also been reported that strain in the upper and lower clamping sites are commonly larger than the overall tendon strain.[69] The presented results might therefore indeed reflect the native mechanical property of the tendon. Overall, the ex vitro tensile test demonstrated that the sensor system was able to accurately record tendon strains during repetitive loading cycles, providing confidence in the ability of the sensor system to quantify strains in MSTs in vivo.

In vivo sensor implantation and dynamic measurement of tendon strains in a sheep model is an important achievement in this study. No previous study has measured in vivo strains in the medial gastrocnemius tendon of sheep during locomotion, and therefore no comparative values are available. However, estimates of MST strains have been reported to be 2.6% in the lateral digital extensor tendon of sheep while trotting [70] (estimated using wired strain gauges); 1.8% in the deep digital flexor tendon of horse hindlimbs when trotting at 1.8–4.8 m s^{-1}[71] (estimated using motion analysis combined with modeling); 8.5% in the superficial digital flexor tendon; and 5.4% in the deep digital flexor tendon of horse forelimbs when trotting at 3.9 m s^{-1}[72] (measured using motion analysis combined with modelling); 4.2% in the superficial digital flexor tendon and 1.7% in the deep digital flexor tendon of horse forelimbs while trotting[73] (measured using wired mercury-in-silastic strain gauges). Thus, the average peak strain of 3.8% measured in this study are well within the range observed in previous studies, and provides further confidence in the proposed system for reliable application in vivo.

Several limitations of the sensor system need to be addressed to improve its applicability for further in vivo scientific and clinical utilization. First, the overall size of the sensor, especially the inductive coil, should be reduced. In addition, the suturing pads disconnected from the sensor body during dissection following our in vivo experiments, and there was small uncertainty whether the sensor body remained fully attached throughout all our in vivo experiments. Clearly, further structural development

to ensure robustness of the sensors to withstand potentially aggressive in vivo environments is required. Here, sensors may need to be hermetically sealed using additional coating techniques during fabrication in order to remain functional in the living body for longer periods. Also, it remained difficult to align the antenna coil of the readout box to the sensor coil in the hindlimb of the sheep. A possible solution is to integrate a magnet within the sensor coil during fabrication, and then align to its in-body position using another magnet externally. Finally, the sensor system can currently only be used to measure axial strains, and the errors associated with complex structures and loading patterns remain unclear.

In conclusion, we present a novel strain sensor and a wireless readout system with the ability to measure in vivo soft tissue strains. The readout system wirelessly excites the sensor and records its oscillatory resonance signal at a distance of up to 10 cm, enabling passive strain sensing of the chipless sensor without the need for an internal power supply. The sensor exhibits an outstanding resolution that allows it to measure changes of 9 µm axial strains. In addition, the measurement reliability of the sensor is not affected after fatigue loading, suggesting that the sensor is reliable for long-term utilization. The sensor had outstanding applicability for strain sensing during ex vivo tendon tensile tests. In vivo sheep implantation and first experimental data suggest that 1) the sensor can successfully measure tendon strain in a freely moving sheep; 2) the in vivo environment does not affect the sensor body and nanowires, but structural failures indicate that further improvements to the connection between the sensor body and suture pads are warranted. Dynamic movement of the body does not affect the sensor integrity. The ability of our sensor system to perform in vivo wireless measurements of MST strains shows great potential for addressing important clinical questions on musculoskeletal loading, such as validating the results of modeling simulations and optimize the musculoskeletal models, pathological mechanisms, and rehabilitation, but also for establishing and monitoring the efficacy of therapies in orthopedics and sports medicine.

4. Experimental Section

Stretchable Capacitor Fabrication: The Au-TiO_2 NWs in the capacitor were synthesized using a method adapted from Tybrandt et al.[74] (Figure 1a–c). Au-TiO_2 NW tracks were patterned using a wax-assisted vacuum filtration method.[33] A wax printer (Xerox ColorQube 8570N) was used to print wax patterns on hydrophilic polyvinylidene fluoride (PVDF) membranes (0.22 µm pore size, Millipore). 2 mL Au-TiO_2 NW solution was filtered through the PVDF membrane before being dried on a hotplate at 45 °C for 10 min. Afterward, the deposited Au-TiO_2 NWs were rinsed in PBS. Then, PDMS (Sylgard 184, curing agent/base weight ratio of 0.15/1) was spin-coated on a salinized wafer at 600 rpm for 30 s and once again dried on a hotplate at 75 °C for 7 min. The PVDF membrane was placed on the PDMS with full contact, and in order to ensure transfer of the NWs, this composite was then placed on a hotplate at 75 °C for a further 11 min with a weight of 750 g on top. Next, the PVDF membrane was peeled off, leaving an Au-TiO_2 NW layer on the PDMS. A 25 µm polyethylene naphthalate foil (Teonex Q51) was used to mask the contact pads in the following steps of spin-coating. A diluted solution of Dragon Skin (DS) silicone rubber (Dragon Skin 10 SLOW, part A/part B weight ratio of 1/1) in heptane (DS/heptane weight ratio of 1/2) was spin-coated (6000 rpm, 30 s) onto the Au-TiO_2 NWs and cured on a hotplate at 75 °C for 60 min. Afterward, a second layer of diluted DS-heptane solution (DS/heptane weight ratio of 2/1) was spin-coated (6000 rpm, 30 s), and using the same procedure described above, a second layer of Au-TiO_2 NWs was transferred on top and once again cured on a hotplate at 75 °C for 60 min. Finally, PDMS was spin-coated (600 rpm, 30 s) to insulate the Au-TiO_2 NWs, and the sample was cured on the hotplate at 75 °C overnight.

LCR Sensor Fabrication: The coil inductor was fabricated by looping a wire (litz wire 7 × 0.04 mm, Cu/Ag50, TW-0, Elektrisola) around a polymethyl methacrylate (PMMA) ring of 33 mm in diameter. Then the coil inductor was bonded to the contact pads of the stretchable capacitor with PDMS-Ag composite (Ag powder: Sigma-Aldrich, length = 2–3.5 µm; Ag/PDMS volume ratio of 0.3/1).[75] Due to the design of the readout box, the LCR sensor was fabricated toward a target RF of 14 MHz for optimal wireless signal quality. In order to determine the number of turns in the coil, the inductance (L) of the coil inductor was calculated based on the target RF (f) and capacitance (C) of the capacitor according to[76]

$$f = \frac{1}{2\pi\sqrt{LC}} \tag{1}$$

The number of turns (N) was thus calculated according to

$$\mathrm{L} = \frac{\mu_r \mu_0 \mathrm{N}^2 \pi \mathrm{r}^2}{\mathrm{l}} \tag{2}$$

where μ_r is the relative permeability of the core; μ_0 is the permeability of free space; r is the coil radius; and l is the coil length.

Two PMMA pads (pad A: 12 × 13 × 2 mm; pad B: 12 × 8 × 2 mm) with four holes in the corners were fabricated using a laser cutter (Trotec Laser, Speedy 300) and bonded to each end of the capacitor using epoxy (UHU Plus Schnellfest Epoxikleber) (Figure 1a). A PMMA mold was fabricated using the laser cutter for casting the sensor exterior in PDMS. The coil inductor and connecting wires were placed in the mold before the PDMS was poured and the composite cured in an oven at 80 °C for 3 h. Finally, a PMMA pad was fabricated using the laser cutter and bonded to the coil inductor using PDMS.

Readout System Development and Data Processing: The wireless readout system (Figure S2, Supporting Information) was composed of a 13.58 MHz quartz oscillator and a power efficient Class E amplifier with output power of 23–27 dBm. The transmitter signal was sent to a printed circuit board loop antenna that resonates at 13.56 MHz, similar to loops used in radio frequency identification readers. After the transmit time of e.g., 20 µs, the transmitter was switched from the antenna to an internal load. At the same time the transmitter antenna takes on the role of an antenna receiver and listens to sensor response signal, oscillating at its self-resonant frequency. The decaying signal lasts only for a couple of µs, depending on the loss mainly in the sensor capacitor. A fast analog-to-digital converter with sampling rate of 40 MHz or higher digitizes the response signal for further digital signal processing. To decompose the frequency spectrum, a FFT (512-point resolution) was applied, where the maximum power amplitude in the spectrum corresponds to the sensor measurement value (Figure 1f). Smart windowing, interpolation techniques, and precise time gating are mandatory for detection with good SNR. ≈900 µs were then required for filtering, amplifying, and transforming the signal from analog to digital, resulting in a sensor sampling frequency of 1024 Hz. During the sampling time, up to eight sensors can be operated using synchronized time division multiple access.

Characterization of Stretchable Capacitor: The electromechanical properties of the stretchable capacitor were evaluated using a tensile testing machine (DO-FB0.5TS, Zwich/Roell) and a LCR meter (Hioki, IM3536) as follows:

1) *Capacitor signal under stretching*: A stretchable capacitor was mounted on the tensile testing machine, and its original length (L_0) was determined by measuring the stretchable region after applying a minimal stretching force of 0.05 N. L_0 was used to calculate the strain and strain rate (50% s^{-1} for all tests) during subsequent tensile testing. The capacitor was positioned at 5% pre-strain in a custom-designed tank and pre-soaked in PBS for 12 h before being pre-conditioned from

5% to 20% strains for 50 cycles. To test its sensitivity, the capacitor was stretched from 5% to 20% with 0.5% strain steps, with 30 s pause at each step. To test its resolution, the capacitor was stretched in increments of ±0.1% strains for ten cycles at sensor strain levels from 5% to 20% in 1% strain steps.

2) *The effect of fatigue on capacitor signal*: After characterizing its sensitivity and resolution, 100 000 cycles of 5%–20% strains were applied to the capacitor before sensitivity and resolution tests were repeated.

Characterization of Wireless LCR Sensor: The wireless sensing capacity of the complete LCR sensor was characterized based on the following experiments:

1) *Sensor electrical properties under stretching*: The LCR sensor was mounted on a custom-designed manual tensile testing device and stretched from 0 to 25% strains. A network analyzer (mRS RADIO SOLUTIONS, miniVNA) was used to quantify the electrical properties of the LCR sensor. The analyzer coil was placed 1 cm above the sensor's coil and a frequency sweep was carried out from 10 to 20 MHz. In addition to the RF of the sensor, F_{High} (the frequency where the absolute value of Rs [the real part of the impedance] is equal to Xs [the imaginary part of the impedance]) and F_{Low} (the frequency where the absolute value of Rs is equal to the opposite of Xs) were measured. The Q-factor of the LCR sensor was calculated as $Q = RF/(F_{High} - F_{Low})$.
2) *Stability of sensor signal in a simulated in vivo environment*: A LCR sensor was submerged in PBS at 37 °C in a custom-designed incubator for 7 d. Before submerging, the RF and Q-factor of the sensor were measured to provide a baseline. The submerged sensor was then measured four times on the first day, and once per day thereafter.

To test the effect of temperature across a range of in vivo possibilities, a LCR sensor was submerged in PBS at room temperature for 12 h. The PBS was then heated from 22 to 45 °C on a hotplate over a period of 30 min using an electronic probe thermometer (DOSTMANN electronic) to track the temperature. Meanwhile, the RF of the sensor was continuously recorded.

1) Sensor *sensitivity and resolution*: A LCR sensor was mounted on the tensile testing machine. After 50 cycles of preconditioning from 0 to 20% strains, the sensitivity (0–25% strains, 1% per step, 30 s pause), and resolution (levels: ±0.1%, ±0.2%, and ±0.5%, pre-strains: 5%, 10%, and 15%, number of cycles: 10) tests were applied in two different conditions: 1) in air and 2) in PBS. The RF of the sensor was measured using the custom-designed readout system throughout the experiment.

Ex Vivo Sensor Measurements of Tendon Strains: A fresh frozen sheep plantaris tendon was mounted on a tensile testing machine (858 Mini Bionix II, MTS, Eden Prairie, MN) by wrapping the ends of the tendon around cylindrical metal abrasive clamps (Figure 3a). The tendon was preloaded to 6.3 N (0.272 MPa × 37.69 mm^2 (cross-sectional area = mass (4.17 g)/(density (1120 kg m^{-3}[77] × $length_{tendon}$ (58.74 mm))) which was used as the reference baseline at zero strain. A LCR sensor was sutured with a slight capacitor pre-strain onto the tendon while the tendon itself was in a straightened but unstretched position. After 20-min rest, the tendon was preconditioned with 0–1% strains at 0.05% s^{-1} for 101 cycles, and with 0–2% strains at 2% s^{-1} for 51 cycles, followed by the formal test (51 cycles of 0–4% strains at 4% s^{-1}). Each cyclic loading condition was followed by 5 min of rest in the slackened position. During testing, the tendon was kept hydrated by spraying a solution of 0.9% sodium chloride in water every 2 min. The RF of the LCR sensor was calibrated to the strain values produced with sonomicrometry crystals aligned with the LCR sensor using linear regression ($y = 28.33x - 0.33$, with y = strain in % and x = RF of the LCR sensor).

In Vivo Sensor Implantation and Measurement: A LCR sensor was calibrated using the same method as the sensor sensitivity measurement described above. The sensor was then gas sterilized using ethylene oxide. Prior to implantation, a sheep (Île-de-France, 37.8 kg) was trained to walk and trot on a treadmill at different speeds and inclination angles. The sheep was motivated with foot pellets provided in between trotting periods. Access to food was stopped 12 h prior to surgery. On the day of surgery, the sheep was sedated with Dexdomitor (0.5 mg mL^{-1} at 0.05 mg kg^{-1}) and Alfaxan (10 mg mL^{-1} at 2 mg kg^{-1}), followed by intubation and preparation of the hindlimb (shaving and cleaning) while maintaining an appropriate level of anesthesia, which was maintained between 0.5% and 2.5% isoflurane as needed. Breathing and heart rate were monitored throughout the procedures and lubricum was applied on the eyes. Sensor implantation was performed in a standard sterile veterinary surgical environment. A skin incision was made on the left hindlimb of the sheep to expose the gastrocnemius-tendon region. The tendon of the medial gastrocnemius was isolated, and the stretchable capacitor of the LCR sensor was sutured on the tendon with a visible pre-strain (≈5%–10%). The coil antenna of the LCR sensor was sutured on subcutaneous tissues. A custom-designed stainless-steel buckle transducer[78] was surgically implanted onto the same tendon distally from the stretchable capacitor to measure the muscle force on the tendon. Veterinary care was overseen by the on-site veterinary team.

Following routing of the wires of the buckle transducer underneath the skin and connecting the wires to a backpack connecter, the skin incision was closed. A subcutaneous injection of Buprenorphine (0.02 mg kg^{-1}) and Metacam (0.05 mg kg^{-1}) was administered (as well as every 12 h thereafter) to reduce postsurgery symptoms. The sheep walked willingly in her pen 2 h following completion of the surgery. Overall, the sheep was given 68 h to recover until there were minimal signs of limping before obtaining experimental data. Following recovery, the sheep trotted willingly on the treadmill at 1.34 m s^{-1} without significant signs of limping, during which tendon strain and muscle force data (sampling frequency 1000 Hz) were recorded. Furthermore, video recordings at 208 Hz of a high-speed camera (Pike F032B, Allied Vision, Stadtroda, Germany) were used to determine the swing and stance phases of the gait cycles. Data of all sensors were synchronized using a light pulse that was visible in the video, where a change in voltage output sent simultaneously to the strain sensor system and buckle transducer system.

Supporting Information

Supporting Information is available from the Wiley Online Library or from the author.

Acknowledgements

The authors would like to thank Dr. Janos Vörös, Head of the Laboratory of Biosensors and Bioelectronics, ETH Zürich, for technical support, access to methods, and use of lab space. The authors would like to thank SENESCYT for financially supporting on the Ph.D. of Dr. Byron Llerena Zambrano. This study was funded by the Swiss National Science Foundation under Project No. 182241; Early postdoc mobility funding from the Swiss National Science Foundation to FMB (187793); The Killam Foundation, the Canada Research Chair program (CIHR); and NSERC (RGPIN-2020-03920).

Open access funding provided by Eidgenossische Technische Hochschule Zurich.

Conflict of Interest

The authors declare no conflict of interest.

Ethics

The Veterinary Sciences Animal Care Committee of the University of Calgary reviewed and approved all procedures included in the Animal Use Protocol (protocol AC19-0098).

Author Contributions

W.R.T., R.K., and C.R.S.: conceptualization; W.R.T., F.S., R.K., P.R., R.G., W.H., T.L., and M.W.S.: methodology; Q.Z., F.M.B., N.C.A., B.L.Z., S.A., V.U.: investigation; Q.Z., F.M.B., N.C.A., C.R.S., S.A., and R.K.: visualization:; W.R.T., W.H., and F.M.B.: funding acquisition; C.R.S.: project administration; W.R.T., W.H., and R.K.: supervision; Q.Z.: writing – original draft; and W.R.T., C.R.S., F.M.B., and N.C.A.: writing – review & editing.

Data Availability Statement

The data that support the findings of this study are available on request from the corresponding author. The data are not publicly available due to privacy or ethical restrictions.

Keywords

biosensors, musculoskeletal biomechanics, soft tissue strains, stretchable electronics, tissue loadings, wireless sensors

Received: December 2, 2022
Revised: March 14, 2023
Published online: April 5, 2023

[1] P. Devita, W. A. Skelly, *Med. Sci. Sports Exercise* **1992**, *24*, 108.
[2] A. A. Amis, G. P. Dawkins, *J. Bone Jt. Surg. Br.* **1991**, *73*, 260.
[3] C. B. Frank, *J. Musculoskeletal Neuronal Interact.* **2004**, *4*, 199.
[4] E. S. Gardinier, K. Manal, T. S. Buchanan, L. Snyder-Mackler, *J. Orthop. Res.* **2013**, *31*, 458.
[5] M. A. Kessler, H. Behrend, S. Henz, G. Stutz, A. Rukavina, M. S. Kuster, *Knee Surg. Sports Traumatol. Arthrosc.* **2008**, *16*, 442.
[6] C. S. Ahmad, L. H. Redler, M. G. Ciccotti, N. Maffulli, U. G. Longo, J. Bradley, *Am. J. Sports Med.* **2013**, *41*, 2933.
[7] N. J. Cronin, G. Lichtwark, *Gait Posture* **2013**, *37*, 305.
[8] O. S. Mian, J. M. Thom, L. P. Ardigo, A. E. Minetti, M. V. Narici, *Acta Physiol.* **2007**, *189*, 57.
[9] Q. Zhang, N. C. Adam, S. H. H. Nasab, W. R. Taylor, C. R. Smith, *Ann. Biomed. Eng.* **2021**, *49*, 7.
[10] B. D. Beynnon, B. C. Fleming, R. J. Johnson, C. E. Nichols, P. A. Renstrom, M. H. Pope, *Am. J. Sports Med.* **1995**, *23*, 24.
[11] B. D. Beynnon, R. J. Johnson, B. C. Fleming, C. J. Stankewich, P. A. Renstrom, C. E. Nichols, *Am. J. Sports Med.* **1997**, *25*, 823.
[12] S. H. H. Nasab, C. R. Smith, P. Schutz, P. Damm, A. Trepczynski, R. List, W. R. Taylor, *Ann. Biomed. Eng.* **2020**, *48*, 1396.
[13] T. Y. Tsai, M. H. L. Liow, Y. Peng, P. Arauz, G. Li, Y. M. Kwon, *J. Orthop. Res.* **2018**, *36*, 3239.
[14] B. Ravary, P. Pourcelot, C. Bortolussi, S. Konieczka, N. Crevier-Denoix, *Clin. Biomech.* **2004**, *19*, 433.
[15] P. Roriz, L. Carvalho, O. Frazao, J. L. Santos, J. A. Simoes, *J. Biomech.* **2014**, *47*, 1251.
[16] B. C. Fleming, B. D. Beynnon, *Ann. Biomed. Eng.* **2004**, *32*, 318.
[17] T. A. Wren, S. A. Yerby, G. S. Beaupre, D. R. Carter, *Clin. Biomech.* **2001**, *16*, 245.
[18] A. Heijne, B. C. Fleming, P. A. Renstrom, G. D. Peura, B. D. Beynnon, S. Werner, *Med. Sci. Sports Exercise* **2004**, *36*, 935.
[19] B. C. Fleming, B. D. Beynnon, P. A. Renstrom, G. D. Peura, C. E. Nichols, R. J. Johnson, *Am. J. Sports Med.* **1998**, *26*, 109.
[20] H. Nagamoto, N. Yamamoto, Y. Shiota, J. Kawakami, T. Muraki, E. Itoi, *JSES Int.* **2017**, *1*, 104.
[21] S. Fukashiro, P. V. Komi, M. Jarvinen, M. Miyashita, *Clin. Biomech.* **1993**, *8*, 25.
[22] S. Edsfeldt, D. Rempel, K. Kursa, E. Diao, L. Lattanza, *J. Hand Surg. Eur.* **2015**, *40*, 705.
[23] A. Erdemir, A. J. Hamel, S. J. Piazza, N. A. Sharkey, *J. Biomech.* **2003**, *36*, 449.
[24] L. Cai, L. Song, P. Luan, Q. Zhang, N. Zhang, Q. Gao, D. Zhao, X. Zhang, M. Tu, F. Yang, W. Zhou, Q. Fan, J. Luo, W. Zhou, P. M. Ajayan, S. Xie, *Sci. Rep.* **2013**, *3*, 3048.
[25] W. L. Hu, X. F. Niu, R. Zhao, Q. B. Pei, *Appl. Phys. Lett.* **2013**, *102*, 083303.
[26] D. J. Cohen, D. Mitra, K. Peterson, M. M. Maharbiz, *Nano Lett.* **2012**, *12*, 1821.
[27] A. D. Valentine, T. A. Busbee, J. W. Boley, J. R. Raney, A. Chortos, A. Kotikian, J. D. Berrigan, M. F. Durstock, J. A. Lewis, *Adv. Mater.* **2017**, *29*, 1703817.
[28] C. Pang, C. Lee, K. Y. Suh, *J. Appl. Polym. Sci.* **2013**, *130*, 1429.
[29] D. A. Kim, S.-K. Ahn, J. Yoon, *Adv. Mater.* **2019**, *4*, 1800739.
[30] C. X. Hou, W., R. Wu, Y. Wang, Q. Xu, X. Y. Liu, W. Guo, *Small* **2019**, *15*, 1805084.
[31] Y. Q. Cai, J. Qin, W. Li, A. Tyagi, Z. Liu, D. Hossain, H. Chen, J.-K. Kim, H. Liu, M. Zhuan, J. You, F. Xu, X. Lu, D. Sun, Z. Luo, *J. Mater. Chem. A* **2019**, *7*, 27099.
[32] M. N. Dakurah, C. Koo, W. Choi, Y. H. Joung, *Int. Neurourol. J.* **2015**, *19*, 133.
[33] F. Stauffer, Q. Zhang, K. Tybrandt, B. L. Zambrano, J. Hengsteler, A. Stoll, C. Trueb, M. Hagander, J. M. Sujata, F. Hoffmann, J. S. Stekhoven, J. Quack, H. Zilly, J. Goedejohann, M. P. Schneider, T. M. Kessler, W. R. Taylor, R. Kung, J. Voros, *Adv. Mater.* **2018**, *3*, 1800031.
[34] R. C. Sun, S. Correia, Y. Chen, C. Xiang, L. Xu, B. Zhan, M. Chen, I. Farrow, F. Scarpa, J. Rossiter, *Adv. Mater.* **2019**, *4*, 1900100.
[35] S. B. Sang, L. H. Liu, A. Q. Jian, Q. Q. Duan, J. L. Ji, Q. Zhang, W. D. Zhang, *Nanotechnology* **2018**, *29*, 255202.
[36] Z. Cui, F. R. Poblete, G. M. Cheng, S. S. Yao, X. N. Jiang, Y. Zhu, *J. Mater. Res.* **2015**, *30*, 79.
[37] H.-Y. C. Chen, A. T. Conn, *IEEE Sens. J.* **2020**, *20*, 7384.
[38] S. Z. Seyedin, P. M. Naebe, S. Yin, J. Chen, X. Wang, J. M. Razal, *Mater. Horiz.* **2019**, *6*, 219.
[39] H. Souri, H. Banerjee, A. Jusufi, N. Radacsi, A. A. Stokes, I. Park, M. Sitti, M. Amjadi, *Adv. Intell. Syst.* **2020**, *2*, 2000039.
[40] M. Amjadi, K. U. Kyung, I. Park, M. Sitti, Stretchable, *Adv. Funct. Mater.* **2016**, *26*, 1678.
[41] C. M. Boutry, Y. Kaizawa, B. C. Schroeder, A. Chortos, A. Legrand, Z. Wang, J. Chang, P. Fox, Z. N. Bao, *Nat. Electron.* **2018**, *1*, 314.
[42] M. Zens, J. Ruhhammer, F. Goldschmidtboeing, P. Woias, M. J. Feucht, H. O. Mayr, P. Niemeyer, *J. Biomech. Eng.* **2014**, *136*, 124504.
[43] C. M. Boutry, Y. Kaizawa, B. C. Schroeder, A. Chortos, A. Legrand, Z. Wang, J. Chang, P. Fox, Z. Bao, *Nat. Electron.* **2018**, *1*, 314.
[44] B. S. Klosterhoff, K. G. Ong, L. Krishnan, K. M. Hetzendorfer, Y. H. Chang, M. G. Allen, R. E. Guldberg, N. J. Willett, *J. Biomech. Eng.* **2017**, *139*, 111004.
[45] T. B. Weydts, L. Brancato, M. A. Soebadi, D. De Ridder, R. Puers, *Sens. Actuators, A* **2018**, *280*, 376.
[46] K. J. Lee, N. Chou, S. Kim, *Sensors* **2018**, *18*, 3955.
[47] J. Lee, S. J. Ihle, G. S. Pellegrino, H. Kim, J. Yea, C. Y. Jeon, H. C. Son, C. Jin, D. Eberli, F. Schmid, B. L. Zambrano, A. F. Renz, C. Forro, H. Choi, K. I. Jang, R. Kung, J. Voros, *Nat. Electron.* **2021**, *4*, 291.
[48] K. Tybrandt, D. Khodagholy, B. Dielacher, F. Stauffer, A. F. Renz, G. Buzsaki, J. Voros, *Adv. Mater.* **2018**, *30*, 1706520.
[49] M. Kaya, T. R. Leonard, W. Herzog, *J. Biomech.* **2006**, *39*, 2752.
[50] C. Y. Liu, Y. G. Dong, *IEEE Sens. J.* **2012**, *12*, 3417.
[51] M. Forouzandeh, N. C. Karmakar, *Wireless Power Transfer* **2015**, *2*, 62.
[52] T. Wang, Z. Lin, R. E. Day, B. Gardiner, E. Landao-Bassonga, J. Rubenson, T. B. Kirk, D. W. Smith, D. G. Lloyd, G. Hardisty, A. Wang, Q. Zheng, M. H. Zheng, *Biotechnol. Bioeng.* **2013**, *110*, 1495.
[53] S. M. Morrison, T. J. Dick, J. M. Wakeling, *J. Biomech.* **2015**, *48*, 3530.
[54] T. Wang, P. Chen, M. Zheng, A. Wang, D. Lloyd, T. Leys, Q. Zheng, M. H. Zheng, *J. Orthop. Res.* **2018**, *36*, 566.

[55] G. A. Johnson, D. M. Tramaglini, R. E. Levine, K. Ohno, N. Y. Choi, S. L. Woo, *J. Orthop. Res.* **1994**, *12*, 796.
[56] G. Hamoir, L. Piraux, I. Huynen, *Microwave Opt. Technol. Lett.* **2012**, *54*, 1633.
[57] E. Siman-Tov, V. F. G. Tseng, S. S. Bedairo, N. Lazarus, *IEEE Trans. Microwave Theory* **2018**, *66*, 5021.
[58] M. Kim, B.-U. Moon, C. H. Hidrovo, *J. Micromech. Microeng.* **2013**, *23*, 095024.
[59] C. N. Maganaris, J. P. Paul, *J. Physiol.* **1999**, *521*, 307.
[60] S. Otsuka, T. Yakura, Y. Ohmichi, M. Ohmichi, M. Naito, T. Nakano, Y. Kawakami, *J. Biomech.* **2018**, *77*, 69.
[61] J. W. Arkwright, N. G. Blenman, I. D. Underhill, S. A. Maunder, M. M. Szczesniak, P. G. Dinning, I. J. Cook, *Opt. Express* **2009**, *17*, 4500.
[62] T. Yamada, Y. Hayamizu, Y. Yamamoto, Y. Yomogida, A. Izadi-Najafabadi, D. N. Futaba, K. Hata, *Nat. Nanotechnol.* **2011**, *6*, 296.
[63] Y. G. Hu, T. Zhao, P. L. Zhu, Y. Zhang, X. W. Liang, R. Sun, C. P. Wong, *Nano Res.* **2018**, *11*, 1938.
[64] R. Rahimi, M. Ochoa, W. Y. Yu, B. Ziaie, *ACS Appl. Mater. Interfaces* **2015**, *7*, 4463.
[65] S. M. Lee, H. J. Byeon, B. H. Kim, J. Lee, J. Y. Jeong, J. H. Lee, J. H. Moon, C. Park, H. Choi, S. H. Lee, K. H. Lee, *BioChip J.* **2017**, *11*, 153.
[66] E. Delivopoulos, D. J. Chew, I. R. Minev, J. W. Fawcett, S. P. Lacour, *Lab Chip* **2012**, *12*, 2540.
[67] A. Srikandakumar, E. H. Johnson, O. Mahgoub, *Small Ruminant Res.* **2003**, *49*, 193.
[68] B. E. Schubert, D. Floreano, *RSC Adv.* **2013**, *3*, 24671.
[69] M. V. Wood, A. Casha, A. Gatt, C. Formosa, N. Chockalingam, J. N. Grima, R. Gatt, *Phys. Status Solidi B* **2019**, *256*, 1800159.
[70] M. Kear, R. N. Smith, *Acta Orthop. Scand.* **1975**, *46*, 896.
[71] A. A. Biewener, *Comp. Biochem. Physiol., Part B: Biochem. Mol. Biol.* **1998**, *120*, 73.
[72] S. E. Lawson, H. Chateau, P. Pourcelot, J. M. Denoix, N. Crevier-Denoix, *J. Anat.* **2007**, *210*, 583.
[73] D. J. Riemersma, A. J. vandenBogert, M. O. Jansen, H. C. Schamhardt, *Equine Vet. J.* **1996**, *28*, 133.
[74] K. Tybrandt, D. Khodagholy, B. Dielacher, F. Stauffer, A. F. Renz, G. Buzsaki, J. Voros, *Adv. Mater.* **2018**, *30*, 1706520.
[75] S. A. Z. Dual, L. B. S. Sündermann, N. Cesarovic, M. Kron, K. Magkoutas, J. Hengsteler, V. Falk, C. Starck, M. Meboldt, J. Vörös, M. S. Daners, *Adv. Healthcare Mater.* **2020**, *9*, 2000855.
[76] S. Charkhabi, Y. J. Chan, D. G. Hwang, S. T. Frey, M. D. Bartlett, N. F. Reuel, *Adv. Mater.* **2019**, *4*, 1800683.
[77] R. F. Ker, *J. Exp. Biol.* **1981**, *93*, 283.
[78] B. Walmsley, J. A. Hodgson, R. E. Burke, *J. Neurophysiol.* **1978**, *41*, 1203.